Dynamic Stall of a Constant-Rate Pitching Airfoil

Miguel R. Visbal*
Wright Research and Development Center, Wright-Patterson AFB, Ohio 45433-6553

A computational study is presented for the dynamic stall of an airfoil that is pitched at a constant rate from zero incidence to a high angle of attack. The unsteady flow is simulated employing the mass-averaged Navier-Stokes equations and an algebraic turbulent eddy viscosity model. The approach is first validated by comparison of computed and experimental results for a pitching airfoil at low freestream Mach numbers. The computed dynamic stall events, as well as the computed effects of pitch rate and axis location, are found in qualitative agreement with experimental observations. The effect of compressibility on dynamic stall is investigated. As the freestream Mach number increases, the appearance of a supersonic region provides—through the shock/boundary-layer interaction—an additional mechanism in the dynamic stall process. The main effects of compressibility are found to be 1) a change from trailing-edge stall to leading-edge stall and 2) a reduction in the stall delay and in the attained maximum lift.

Nomenclature

C_L, C_D, C_M	= lift, drag, and quarter-chord moment coefficients
C_p	= pressure coefficient, $2(p-p_\infty)/\rho_\infty U_\infty^2$
c	= airfoil chord
M	= Mach number
n	= direction normal to airfoil surface
p	= pressure
Re_c	= chord Reynolds number, $\rho_\infty U_\infty c/\mu_\infty$
T	= temperature
t	= time
t^+	= nondimensional time, $= tU_\infty/c$
U	= velocity vector
u, v	= Cartesian velocity components in inertial frame of reference
X, Y	= coordinate system attached to airfoil (see Fig. 1)
X_0	= pitch-axis location
x, y	= Cartesian coordinates in inertial frame of reference
α	= geometric angle of attack
$\alpha_{C_{L_{max}}}, \alpha_{C_{D_{max}}}$	= angles at maximum lift and drag, respectively
ξ, η, τ	= transformed coordinates
Ω	= airfoil pitch rate, rad/s
Ω^+	= nondimensional pitch rate, $\Omega c/U_\infty$

Subscripts

max, min	= maximum and minimum values
∞	= freestream conditions

I. Introduction

WHEN airfoils or wings are rapidly pitched beyond their static-stall angle, the disparities in the time scales associated with inviscid and viscous phenomena permit an angular delay of stall and an aerodynamic lift temporarily higher than the static stall situation. This complex, unsteady flow process, denoted in general as dynamic stall, has been the subject of numerous investigations.[1-3]

The majority of the research on dynamic stall has been motivated by its application to helicopter retreating-blade stall and has concentrated on airfoils subjected to sinusoidal pitch oscillations of moderate rate and amplitude. Recently, however, projected aircraft maneuverability enhancements[4] have stimulated interest in the case of constant-rate, high-amplitude pitch motion, as evidenced by the experiments in Refs. 5-12 and the computational work of Refs. 13-15. The study of constant-rate pitching, starting from a well-defined steady flow condition, is also attractive because it allows the investigation of dynamic stall without the added complexity of motion history effects. Even for this simple type of forced motion, progress in understanding and prediction of dynamic stall is hindered by the need to account for many, often interrelated, flow effects[1,2]; for example, compressibility, Reynolds number dependence, pitch-rate and pitch-axis location, as well as three dimensionality and wing or airfoil geometric effects. In particular, little is known about compressibility and three-dimensional dynamic stall effects, both of which are important in rapidly maneuvering aircraft. Even at relatively low freestream Mach numbers ($M_\infty \gtrsim 0.2$), compressibility can significantly affect dynamic stall behavior[16] because high local Mach numbers occur on a pitching airfoil due to the delay of stall. Once transonic flow develops, its associated normal shock provides, by means of the shock-wave/boundary-layer interaction, an additional mechanism in the dynamic stall process. Except for the study of Lorber and Carta[6] and the recently initiated work of Bodapati and Carr,[17] experiments on

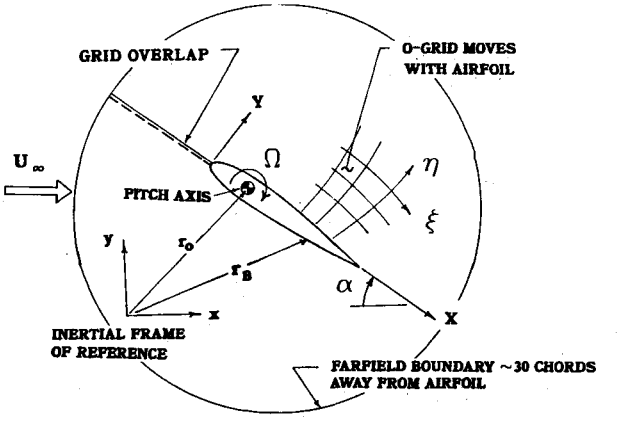

Fig. 1 Pitching airfoil configuration.

Presented as Paper 88-0132 at the AIAA 26th Aerospace Sciences Meeting, Reno, NV, Jan. 11-14, 1988; received May, 9, 1989; revision received Nov. 20, 1989.

*Aerospace Engineer. Member AIAA.

constant-rate pitching airfoils have been conducted at very low freestream Mach numbers ($M_\infty < 0.1$). Further systematic experimental and computational investigations are therefore required in order to elucidate the effect of compressibility on dynamic stall.

After the preceding brief background, the objectives of the present investigation of dynamic stall are summarized as follows:

1) Extension of the author's previous laminar study[14] for constant-rate pitching airfoils to the more realistic case of high Reynolds number flow employing an algebraic eddy viscosity model.[18]

2) Investigation of the effects of pitch rate and pitch-axis location on the dynamic stall process.

3) Study of the influence of compressibility on the dynamic stall of a constant-rate pitching airfoil.

To accomplish these objectives, computations were performed for the flow configuration depicted in Fig. 1. A NACA 0015 airfoil was pitched about a fixed axis and at a constant rate from zero incidence to a high angle of attack. The freestream Mach number and chord Reynolds number varied over the ranges 0.2–0.6 and 2×10^5–1×10^6, respectively. The nondimensional pitch rate Ω^+ ranged from 0.02 to 0.4, and different pitch-axis locations were also considered. Numerical results were obtained by solving the unsteady, compressible, mass-averaged Navier-Stokes equations using an implicit algorithm[19] and an algebraic eddy viscosity turbulence model.[18]

II. Method of Solution

Governing Equations and Boundary Conditions

For the case of external flow past a body in arbitrary motion, the governing equations can be formulated in an inertial frame of reference, and motion of the body can be provided for by means of a general time-dependent coordinate transformation. Introducing such a transformation [$\xi=\xi(x,y,t)$, $\eta=\eta(x,y,t)$, $\tau=t$], the full two-dimensional, compressible Navier-Stokes equations may be expressed in the following strong-conservation form[20]:

$$\partial_\tau q+\partial_\xi E_1+\partial_\eta E_2=\partial_\xi(V_1+V_2)+\partial_\eta(W_1+W_2) \qquad (1)$$

where $q=J^{-1}(\rho,\rho u,\rho v,\rho e)^T$ is the vector of dependent variables. The form of the flux vectors appearing in Eq. (1) can be found in Ref. 20. Closure of this system of equations is provided by the perfect gas law, Sutherland's viscosity formula, and the assumption of a constant molecular Prandtl number. Turbulence is simulated employing mass-averaged variables[21] and the algebraic eddy viscosity model of Baldwin and Lomax.[18]

In reference to the pitching airfoil configuration shown in Fig. 1, the boundary conditions are prescribed as follows. Along the inflow portion of the farfield boundary, freestream conditions are specified. First-order extrapolation is used on the outflow boundary for all flow variables. Along the 0-grid cut, spatial periodicity is imposed in the ξ direction by means of a grid overlap. On the airfoil surface, the following adiabatic, no-slip condition is applied

$$U=U_B \qquad \frac{\partial T}{\partial n}=0 \qquad \frac{\partial p}{\partial n}=-\rho a_B\cdot\hat{n} \qquad (2)$$

where U_B and a_B denote, respectively, the velocity and acceleration on the airfoil surface and are given by

$$U_B=\Omega\times(r_B-r_0) \qquad (3a)$$

$$a_B=d\Omega/dt\times(r_B-r_0)-\Omega^2(r_B-r_0) \qquad (3b)$$

for the case of rotation about a fixed axis (see Fig. 1).

Finally, the formulation of the problem is completed by imposing as an initial condition the computed flow at 0-deg angle of attack. In addition, at the onset of rotation, the airfoil accelerates to its final constant pitch rate as described in Ref. 13.

Numerical Procedure

The time-dependent coordinate transformation (i.e., moving grid) required in the present flow simulation is implemented using a rigid grid attached to the airfoil. This approach is employed because it eliminates the need for multiple grid generation. A nearly orthogonal, boundary-fitted 0-grid is generated about the airfoil employing the elliptic technique of Ref. 22. The grid extends 30 chords away from the airfoil and has minimum spacings of $0.00075c$ and $0.00001c$ in the ξ and η directions, respectively.

The governing equations are numerically solved employing the implicit approximate-factorization algorithm of Beam and Warming.[19] This scheme is formulated using three-point, backward time differencing and second-order centered approximations for all spatial derivatives. In order to control numerical stability, both explicit and implicit smoothing terms are added to the basic algorithm. A fully vectorized Navier-Stokes solver that employs the preceding scheme has been developed and successfully validated for a variety of both steady and unsteady flow problems.[13,14,23] A nondimensional time step $\Delta t^+=0.002$ is specified in all of the present dynamic stall calculations.

III. Results and Discussion

Before proceeding to the case of dynamic stall, computations were performed for a stationary airfoil in order to test the implementation of the turbulence model. Calculations were done for a NACA 0012 at various angles of attack and for a freestream Mach number and chord Reynolds number of 0.6 and 3×10^6, respectively. The transition location on the airfoil upper surface was specified at $X/c=0.05$, as fixed in the experiments of Ref. 24. Figure 2 shows a good agreement between the computed and the experimental lift coefficient vs corrected[24] angle of attack (α_c). A comparison of the computed and measured pressure distributions is given in Fig. 3 for $\alpha_c=6.48$ deg. The excellent prediction of C_p achieved for this supercritical case using a simple algebraic turbulence model is expected only in the absence of substantial shock-induced boundary-layer separation.[25]

Dynamic Stall Results at $M_\infty=0.2$

One of the objectives of this investigation is the extension of the author's previous work[14] on laminar flow past a pitching airfoil to the more realistic case of high Reynolds number turbulent flow using an algebraic eddy viscosity model. To achieve this objective, computations were performed for a

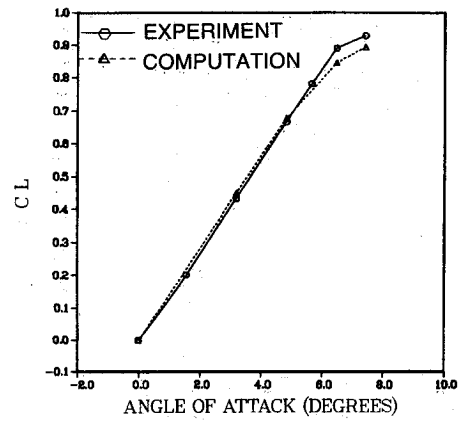

Fig. 2 Comparison of computed and experimental[24] lift coefficients (NACA 0012, $M_\infty=0.6$, $Re_c=3\times10^6$).

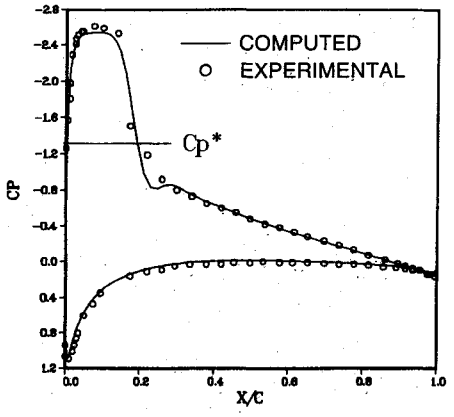

Fig. 3 Comparison of computed and experimental[24] C_p (NACA 0012, $\alpha_c = 6.48$ deg, $M_\infty = 0.6$, $Re_c = 3 \times 10^6$).

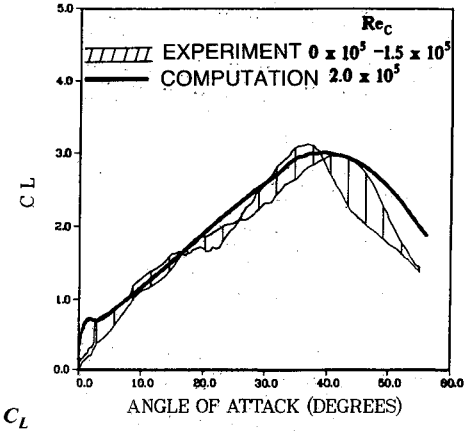

a) C_L

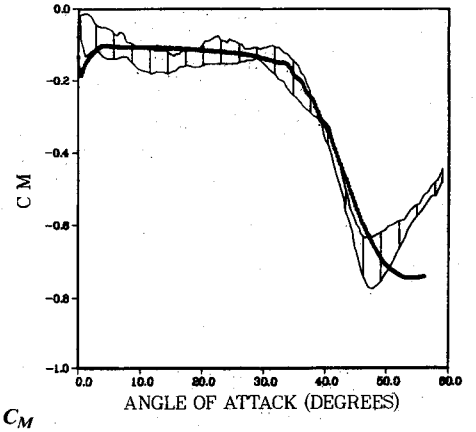

b) C_M

Fig. 4 Comparison of computed and experimental[10] aerodynamic coefficients ($\Omega^+ = 0.2$, $X_0/c = 0.25$).

NACA 0015 airfoil that was pitched at a constant rate and about a fixed axis (see Fig. 1) from 0-deg angle of attack to a high incidence beyond the static stall angle. The freestream Mach number and the chord Reynolds number were 0.2 and 2×10^5, respectively. The nondimensional pitch rate $\Omega^+ = \Omega c/U_\infty$ ranged from 0.02 to 0.4, and different pitch axis locations were also considered. In all calculations, the transition location on the airfoil upper surface was held fixed at the leading edge, simulating the case of an airfoil with a boundary-layer trip. Simulation of the practical case of natural transition was not attempted in the present numerical study due to the following reasons. First, for the specific airfoil section and flow parameters investigated, no experimental unsteady transition data are available for comparison. Second, experiments[26] for a NACA 0012 airfoil subjected to sinusoidal pitch oscillations revealed no changes in the basic dynamic stall characteristics when a boundary-layer trip was placed at the leading edge. The experiments of Refs. 6 and 26 indicate that, for sufficiently high Reynolds number, the stall process is associated with turbulent boundary-layer separation rather than with the bursting of the leading-edge laminar separation bubble. As discussed in Ref. 27, however, the effects of transition on unsteady flows are very important, and detailed experimental studies on the influence of transition of dynamic stall are required for guidance in numerical simulation.

Description of the Dynamic Stall Process for $\Omega^+ = 0.2$

Only the case when $\Omega^+ = 0.2$ and $X_0/c = 0.25$ is discussed in detail in this section. A comparison of the computed and experimental[10] lift and moment coefficients is shown in Fig. 4. The agreement between the calculated and measured aerodynamic coefficients is reasonably good. The present numerical approach with an algebraic turbulence model is capable of predicting the measured levels of $C_{L_{max}}$ and $C_{M_{min}}$, as well as the initiation of moment stall and the angle of maximum lift. However, discrepancies between the computed and experimental C_L and C_M distributions are apparent in the poststall regime ($\alpha > 45$ deg in Figs. 4a and 4b). These discrepancies may be associated with deficiencies in the turbulence model and/or with three-dimensional effects present in the experiments. Given the uncertainties in the turbulence model for massively separated flowfields, emphasis in the paper is placed on the prediction of the onset of dynamic stall.

The flowfield evolution is presented in Figs. 5 and 6 in terms of instantaneous streamlines (relative to the airfoil frame of reference) and of the airfoil upper surface pressure distributions. As the airfoil incidence increases, a trailing-edge reversed-flow region appears, which grows in size and propagates at an increasing rate toward the leading edge (see Figs. 5a and 5b). A major portion of this separation region is, however, very thin, and the outer inviscid flow remains parallel to the airfoil surface for most of its length. During this separation stage, the flowfield is also characterized by 1) the aft displacement of the stagnation point along the airfoil lower surface (see Figs. 5a and 5b), 2) a rapid increase in the leading-edge suction peak (see Fig. 6a), 3) a fairly linear

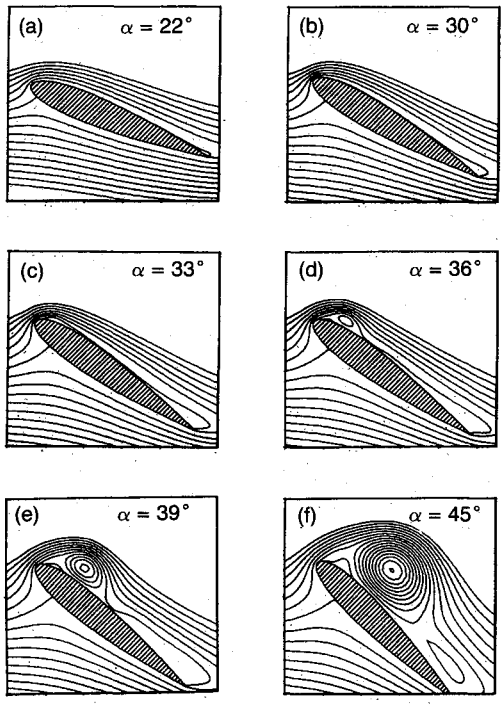

Fig. 5 Flowfield evolution ($\Omega^+ = 0.2$, $X_0/c = 0.25$, $M_\infty = 0.2$, $Re_c = 2 \times 10^5$).

$C_L - \alpha$ relation (see Fig. 4a), and 4) a nearly constant (nose-down) moment coefficient (see Fig. 4b).

With the continuous increase in incidence, separation eventually reaches the vicinity of the airfoil leading edge and the highest level of the leading-edge suction peak ($C_{p_{min}}$) is attained. Because the rate at which suction develops decreases at this stage, a temporary slight reduction in the lift-curve slope occurs (see Fig. 7). This reduction in $dC_L/d\alpha$, which becomes more apparent for smaller Ω^+ (see Fig. 7), is also observed in the experiments of Refs. 6 and 7. The forward propagation of the separation region halts as it approaches the airfoil leading edge (at $\alpha \approx 31$ deg). Subsequently, the separation streamline departs from the surface at an increasing angle (with respect to the airfoil chord) and then rapidly turns toward the airfoil surface (see Fig. 5c). This event manifests itself as the vortex-induced suction peak in the C_p distribution (see Fig. 6a). As the vortex-induced suction develops, the lift continues to increase at a faster rate (i.e., $dC_L/d\alpha$ increases again; see Fig. 7). However, moment stall occurs as leading-edge suction collapses (see Fig. 6b) and the vortex moves downstream. The subsequent flowfield evolution is basically characterized by the downstream displacement of the leading-edge vortex (see Figs. 5d–5f), also evident from the airfoil upper surface pressure distribution (see Fig. 6b). These calculated results are in qualitative agreement with experimental observations.[7,10]

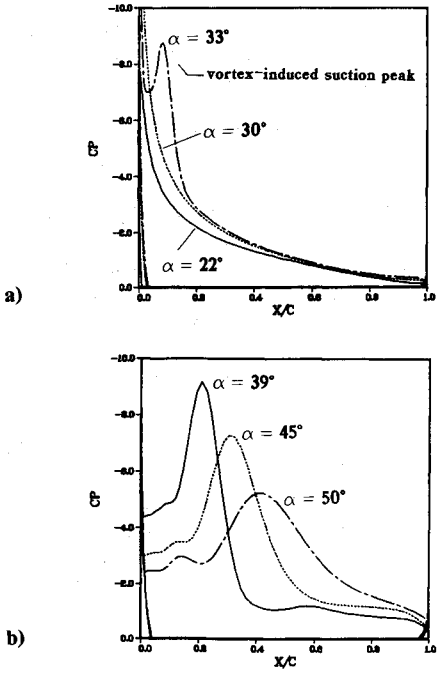

Fig. 6 Airfoil upper surface pressure distribution ($\Omega^+ = 0.2$, $X_0/c = 0.25$, $M_\infty = 0.2$, $Re_c = 2 \times 10^5$).

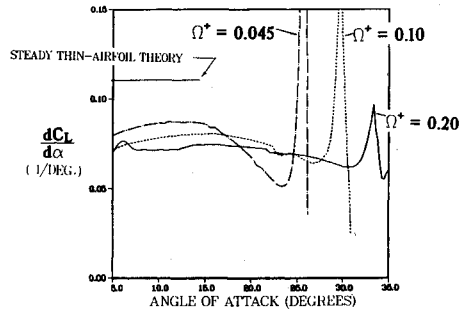

Fig. 7 Effect of Ω^+ on lift-curve slope history ($X_0/c = 0.25$, $M_\infty = 0.2$, $Re_c = 2 \times 10^5$).

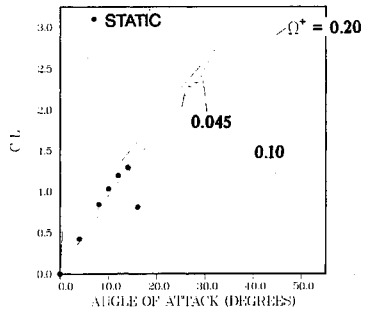

Fig. 8 Effect of Ω^+ on lift coefficient history ($X_0/c = 0.25$, $M_\infty = 0.2$, $Re_c = 2 \times 10^5$).

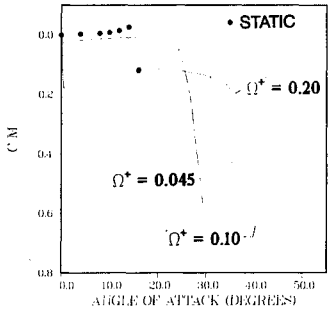

Fig. 9 Effect of Ω^+ on moment coefficient history ($X_0/c = 0.25$, $M_\infty = 0.2$, $Re_c = 2 \times 10^5$).

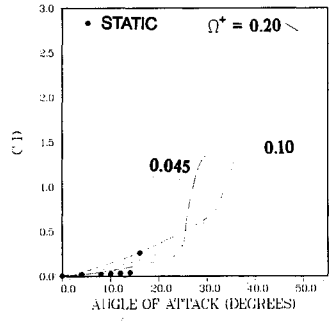

Fig. 10 Effect of Ω^+ on drag coefficient history ($X_0/c = 0.25$, $M_\infty = 0.2$, $Re_c = 2 \times 10^5$).

Effects of Pitch Rate and Pitch-Axis Location

To investigate the effect of pitch rate on dynamic stall, calculations were performed for a NACA 0015 airfoil pitching at various values of Ω^+ over the range 0.02–0.4. The pitch-axis location was fixed at $X/c = 0.25$ and the freestream Mach number and Reynolds number were 0.2 and 2×10^5, respectively.

Detailed examination of the computed flowfields indicated that over the Ω^+ range 0.045–0.4, the qualitative features of the dynamic stall process remained essentially the same. This process was characterized by the propagation of the trailing-edge separation region toward the airfoil leading edge and by the formation of a dynamic stall vortex that was convected downstream over the airfoil. However, the computed results for the lowest pitch rate ($\Omega^+ = 0.02$) did not display the same dynamic stall features. Instead of the formation of a leading-edge vortex, the trailing-edge separation region evolved into massive separation on the airfoil leeward side. A transition from dynamic to static-stall behavior is expected to occur as Ω^+ decreases. However, the experimental work of Ref. 7 indicates that the typical dynamic stall features are still present for values of Ω^+ as low as 0.01. The computed behavior for $\Omega^+ = 0.02$, which is apparently in disagreement with ex-

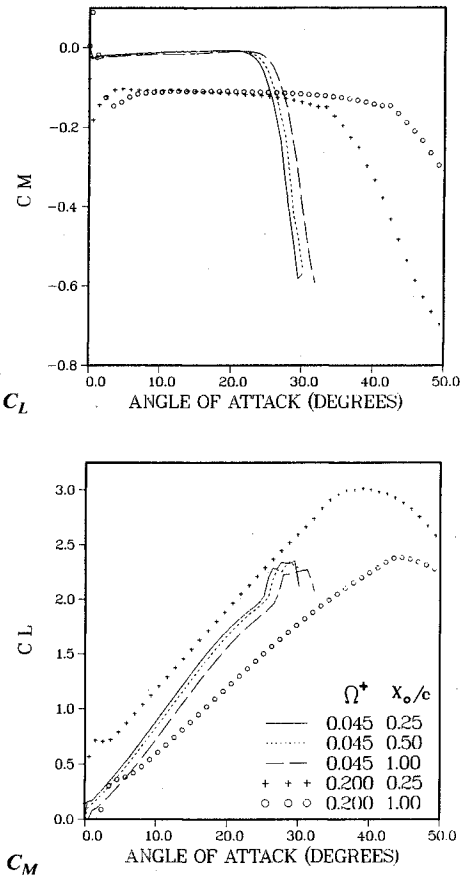

Fig. 11 Effect of pitch-axis location on aerodynamic coefficient histories ($M_\infty = 0.2$, $Re_c = 2 \times 10^5$).

perimental observations, can perhaps be attributed to limitations of the present turbulence model.

The aerodynamic coefficient histories are shown in Figs. 8–10 for three different values of Ω^+. The corresponding computed airfoil static loads are also included in these figures for the purpose of comparison. The most important effects of pitch rate can be summarized as follows.

1) Increasing Ω^+ produces an angular delay of the dynamic stall process as evident, for instance, from the angle at which $C_{L\max}$ occurs (see Fig. 8).

2) Increasing Ω^+ results in higher values of $C_{L\max}$, $C_{D\max}$, and $|C_{M\min}|$ (see Figs. 8–10).

3) At the onset of rotation, the airfoil lift coefficient (see Fig. 8) displays a sudden increase or jump that is approximately proportional to the pitch rate. In addition, the slope of the linear portion of the C_L curve decreases with Ω^+ (see Figs. 7 and 8).

The preceding pitch-rate effects and trends are in agreement with experimental observations.[6,7] In particular, the computed C_L-jump and lift-curve slope depression [3) above] are in line with the inviscid theoretical predictions of Ref. 7.

The influence of the pitch-axis location on the dynamic stall phenomena was also investigated for two different values of Ω^+ (see Fig. 11). For both pitch rates, displacement of the pivot axis downstream (along the airfoil chord) resulted in a further delay of dynamic stall. The stall delay produced by a given pivot-axis displacement is more pronounced at higher values of Ω^+. The angular delay ($\Delta\alpha$) in the initiation of moment stall (see Fig. 11b) can be approximated by $\Delta\alpha(\text{rad}) = \Omega^+ \Delta(X_0/c)$, where $\Delta(X_0/c)$ denotes the shift in the pivot-axis location. This linear expression for $\Delta\alpha$ is nothing more than the motion-induced difference in effective angle of attack at the airfoil leading edge (for small α). For the case of $\Omega^+ = 0.2$, the aft displacement of the pitch axis produced a substantial reduction in $C_{L\max}$ (see Fig. 11a). However, for $\Omega^+ = 0.045$, $C_{L\max}$ varied considerably less with pitch-axis position. In fact, the lift and moment curves for the different pivot locations for $\Omega^+ = 0.045$ can be almost matched by a simple shift in angle of attack ($\Delta\alpha$). This small effect of axis location at low Ω^+ should permit the correlation of experimental data obtained for the same pitch rate but with different pivot locations. The predicted stall delay caused by the aft displacement of the rotation axis is in agreement with the experimental work of Refs. 8 and 9 and with the author's previous laminar computations.[14]

Compressibility Effects

The experiments of Ref. 16 for several airfoil sections in sinusoidal pitch oscillations indicated the development of sonic conditions near the leading edge for $M_\infty \gtrsim 0.2$. Reference 6 also reported the presence of a supersonic region near the leading edge of an airfoil at constant pitch rate and $M_\infty = 0.4$. The turbulent computations described in the preceding section for a NACA 0015 airfoil with $\Omega^+ = 0.2$ and $M_\infty = 0.2$ indicated a maximum instantaneous local Mach number $M_{\max} \cong 0.9$. These high local Mach numbers attained by pitching airfoils in low subsonic streams result from the dramatic delays of leading-edge separation to high angles of attack. The maximum local value of Mach number is therefore dependent not only on M_∞ and leading-edge geometry but also on the nondimensional pitch rate. The appearance of a supersonic region, which usually terminates in a normal shock, provides—by means of the shock/boundary-layer interaction—an additional mechanism in the dynamic stall process.

To investigate the effect of compressibility on dynamic stall, computations were performed for a pitching NACA 0015 airfoil at different freestream Mach numbers (namely 0.2, 0.3, 0.4, 0.5, and 0.6). The chord Reynolds number was 10^6, Ω^+ was varied from 0.02 to 0.4, and the pitch-axis location was at $X/c = 0.25$. In all cases, transition was fixed at the airfoil leading edge.

Fully Developed Supercritical Flow

For freestream Mach numbers $M_\infty = 0.5$ and 0.6, the flowfield structure about the pitching airfoil displayed the features of a supercritical flow. The main flow events observed at high Mach numbers are described for the case of $M_\infty = 0.6$ and $\Omega^+ = 0.045$. As the angle of attack increases, a well-defined

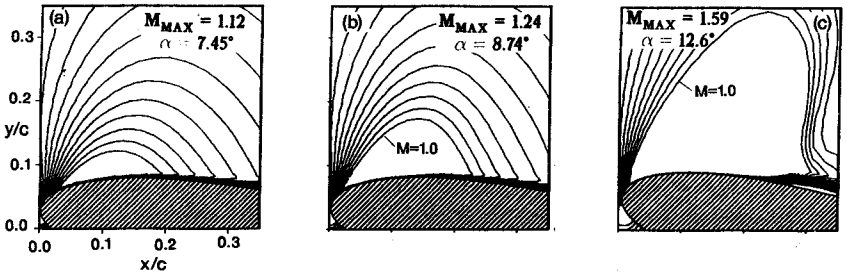

Fig. 12 Evolution of supersonic region ($\Omega^+ = 0.045$, $M_\infty = 0.6$, $Re_c = 1 \times 10^6$).

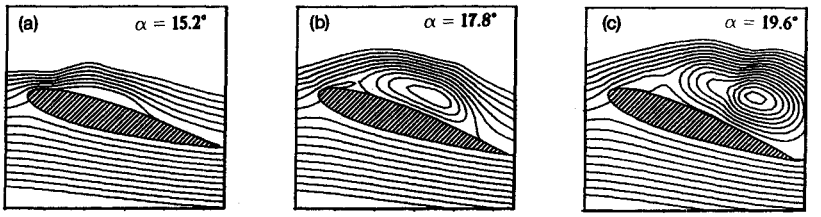

Fig. 13 Evolution of relative streamlines ($\Omega^+ = 0.045$, $M_\infty = 0.6$, $Re_c = 1 \times 10^6$).

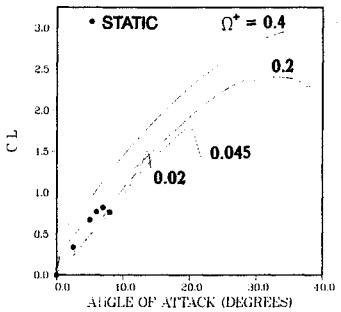

Fig. 14 Effect of Ω^+ on lift coefficient history ($M_\infty = 0.6$, $Re_c = 1 \times 10^6$).

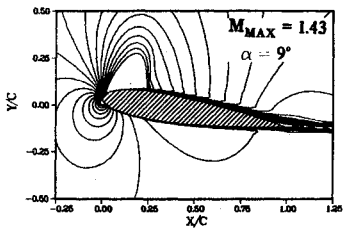

a) $\Omega^+ = 0.02$

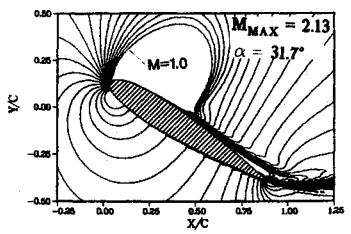

b) $\Omega^+ = 0.4$

Fig. 15 Effect of Ω^+ on the extent of the supersonic region ($M_\infty = 0.6$, $Re_c = 1 \times 10^6$).

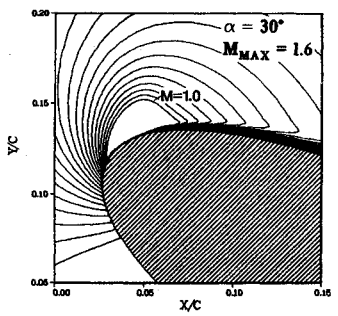

Fig. 16 Development of transonic flow near airfoil leading edge ($M_\infty = 0.3$, $\Omega^+ = 0.4$, $Re_c = 1 \times 10^6$).

supersonic region develops on the airfoil upper surface, as shown in Fig. 12. Due to the severe adverse pressure gradients induced by the shock, boundary-layer separation occurs (see Fig. 13a). The separation region that originates at the foot of the shock propagates both upstream and downstream over the airfoil surface as the angle of attack continues to increase. When separation reaches the vicinity of the leading edge, the turning of the inviscid flow (around the airfoil nose) decreases, the leading edge suction level rapidly drops, and moment stall begins. Subsequently, massive separation is observed on the airfoil upper surface (see Fig. 13c) and lift stall also occurs.

Figures 14 and 15 illustrate the effects of Ω^+ on the pitching airfoil flow for $M_\infty = 0.6$. As in the case of low Mach number, increasing the pitch rate results in a larger angular delay of dynamic stall and in higher values of maximum lift (see Fig. 14). From Fig. 14, one can also observe that the C_L jump that occurs at the onset of rotation at low freestream Mach number (see Fig. 8) is considerably reduced by compressibility effects. Examination of the flowfield before significant separation has yet occurred (see Fig. 15) indicates that as Ω^+ increases a higher local $M_{\max}$ is obtained over the airfoil upper surface. As a consequence, the extent of the supersonic region increases and the normal shock is located further downstream. From the present results, it is apparent that for $M_\infty = 0.6$ the dynamic stall process is controlled by the shock/boundary-layer interaction. Given the uncertainties involved in turbulence modeling of such complex phenomena, experimental work is required to provide quantitative information on dynamic stall at high subsonic Mach numbers. Some of the aspects of unsteady, shock-induced separation have been discussed by Ericsson.[28]

Dynamic Stall at Intermediate Mach Numbers ($M_\infty = 0.3, 0.4$)

Even for a freestream Mach number as low as 0.3, a supersonic region is observed to develop on the airfoil upper surface (see Fig. 16). Although this supersonic bubble is very limited in chordwise extent (approximately 3.0% chord), its appearance indicates the importance of compressibility effects on dynamic stall beginning at relatively low M_∞.

The evolution of the flowfield for $M_\infty = 0.4$ and $\Omega^+ = 0.045$ is shown Fig. 17 by means of instantaneous streamlines. Similar to the low Mach number case, the dynamic stall process is characterized by the formation of a leading-edge vortex that is convected over the airfoil upper surface. However, for $M_\infty = 0.4$, the dynamic stall vortex appears at a much earlier time than when $M_\infty = 0.2$, as shown in Fig. 18. This fact suggests that compressibility must affect the initial boundary-layer separation process that precedes the vortex formation. Indeed, close examination of the flowfield indicated that separation near the leading edge resulted from the shock/boundary-layer interaction and not from the upstream propagation of the trailing-edge separation region. This important qualitative change from trailing-edge stall to leading-edge stall, as M_∞ increases, is in agreement with the experimental work of Ref. 16. Figure 19 shows the evolution of the supersonic bubble during the process of leading-edge separation. The sonic line moves downstream along the airfoil upper surface as the

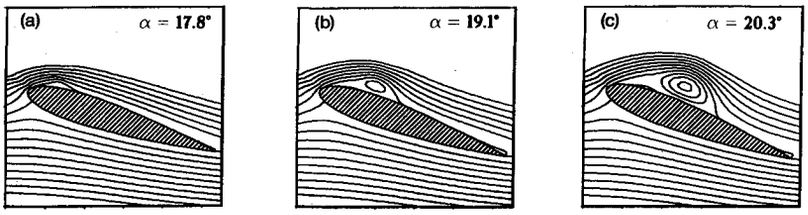

Fig. 17 Evolution of relative streamlines ($M_\infty = 0.4$, $\Omega^+ = 0.045$, $Re_c = 1 \times 10^6$).

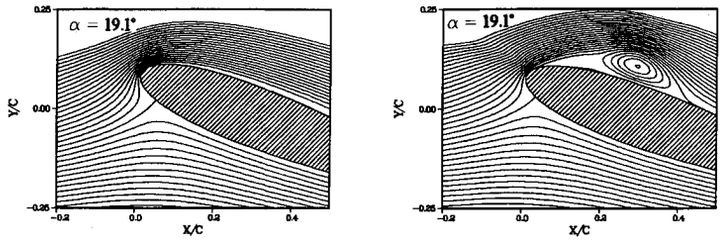

a) $M_\infty = 0.2$ b) $M_\infty = 0.4$

Fig. 18 Effect of compressibility on leading-edge vortex formation ($\Omega^+ = 0.045$, $Re_c = 1 \times 10^6$, $t^+ = 7.5$).

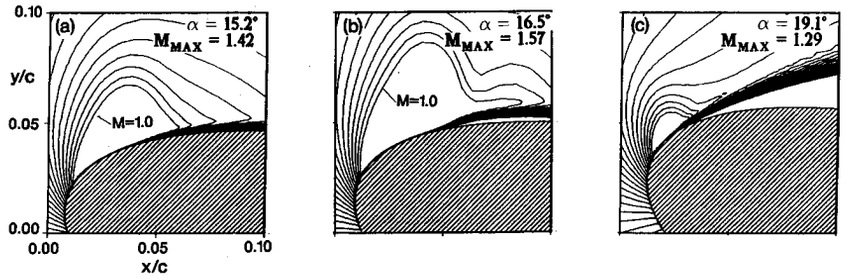

Fig. 19 Evolution of leading-edge supersonic bubble ($M_\infty = 0.4$, $\Omega^+ = 0.045$, $Re_c = 1 \times 10^6$).

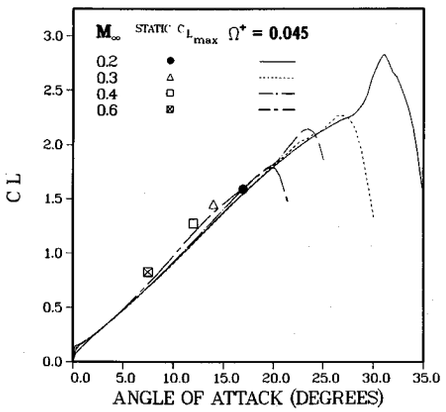

Fig. 20 Effect of compressibility on lift coefficient history ($\Omega^+ = 0.045$, $Re_c = 1 \times 10^6$).

supersonic region develops. After separation, the shock moves upstream and the supersonic zone reduces to a chordwise extent of less than 1.5%. The influence of numerical resolution on the supersonic bubble formation should be further investigated. In addition, experimental flow visualizations of the leading-edge supersonic region are required.

The effect of compressibility on the computed lift coefficient is shown in Fig. 20 for $\Omega^+ = 0.045$ and for different freestream Mach numbers. The corresponding static values of $C_{L_{\max}}$ are also included for comparison. As M_∞ increases, the dynamic stall delay is reduced and $C_{L_{max}}$ decreases. This trend is in agreement with the experiments of Ref. 6. As expected, much of the compressibility effects are already present in the static characteristics. However, some of the reduction in the stall delay is dynamic in nature. For instance, the overshoot in $\alpha_{C_{L\max}}$ decreases from 14 deg at $M_\infty = 0.2$ to 10 deg at $M_\infty = 0.6$.

IV. Conclusions

The turbulent flow about a constant-rate pitching airfoil was numerically simulated employing the mass-averaged, Navier-Stokes equations and an algebraic eddy viscosity turbulence model.

At $M_\infty = 0.2$ and over a wide range of pitch rates ($0.045 \le \Omega^+ \le 0.4$), the computed unsteady flow features were found in qualitative agreement with experimental observations. The dynamic stall process was characterized by forward propagation of the trailing-edge separation region and by the formation of a leading-edge vortex that was convected over the airfoil. For the case of $\Omega^+ = 0.2$, the computed lift and moment coefficient histories were found to be in good quantitative agreement with available experimental data. The effects of pitch rate and pitch-axis location were also investigated and found to be in agreement with experimental observations and with previously computed laminar results. However, the simple eddy viscosity model seems to be inadequate at very low pitch rates because computed results for $\Omega^+ = 0.02$ did not display the basic dynamic stall features.

Compressibility effects on dynamic stall were investigated by varying the freestream Mach number from 0.2 to 0.6. For $M_\infty = 0.5$ and 0.6, a fully developed supercritical flow was observed over the airfoil. Increasing Ω^+ resulted in 1) an increased angular stall delay, 2) higher lift coefficients, 3) higher Mach numbers on the airfoil upper surface, and 4) the displacement of the shock toward the trailing edge. At these high Mach numbers, the dynamic stall process is controlled by the shock/boundary-layer interaction rather than by the formation of a leading-edge vortex. Given the uncertainties involved in the turbulence modeling of such phenomena, detailed experimental studies at high subsonic Mach numbers are required.

At $M_\infty = 0.3$ and 0.4, the flow was supercritical. However, the supersonic region was very limited in spatial extent. The dynamic stall process was still characterized by the formation and convection of a leading-edge vortex. At these intermediate values of M_∞, the main effects of compressibility were 1) a change from trailing-edge stall (observed at $M_\infty = 0.2$) to leading-edge stall, and 2) a decrease in the stall delay and in the maximum lift coefficient. Both of these effects are in qualitative agreement with experimental observations.

References

[1]McCroskey, W. J., "Unsteady Airfoils," *Annual Review of Fluid Mechanics,* Vol. 14, 1982, pp. 285–311.

[2]Carr, L. W., "Progress in Analysis and Production of Dynamic Stall," *Journal of Aircraft,* Vol. 25, Jan. 1988, pp. 6–17.

[3]Ericsson, L. E. and Reding, J. P., "Unsteady Airfoil Stall, Review and Extension," *Journal of Aircraft,* Vol. 18, No. 8, 1971, pp. 609–616.

[4]Lang, J. D. and Frances, M. S., "Unsteady Aerodynamics and Dynamic Aircraft Maneuverability," AGARD Symposium on Unsteady Aerodynamics—Fundamentals and Applications to Aircraft Dynamics, AGARD, Göttingen, Germany, May 1985.

[5]Francis, M. S. and Keesee, J. E., "Airfoil Dynamic Stall Performance with Large-Amplitude Motions," *AIAA Journal*, Vol. 23, No. 11, 1985, pp. 1653–1659.

[6]Lorber, P. F. and Carta, F. O., "Airfoil Dynamic Stall at Constant Pitch Rate and High Reynolds Number," AIAA Paper 87-1329, June 1987.

[7]Jumper, E. J., Shreck, S. J., and Dimmick, R. L., "Lift-Curve Characteristics for an Airfoil Pitching at Constant Rate," *Journal of Aircraft,* Vol. 24, No. 10, 1987, pp. 680–687.

[8]Jumper, E. J., Dimmick, R. L., and Allaire, A. J. S., "The Effect of Pitch Location on Dynamic Stall," *ASME Forum on Unsteady Flow Separation,* FED-Vol. 52, edited by K. N. Ghia, June 1987.

[9]Helin, H. E. and Walker, J. M., "Interrelated Effects of Pitch Rate and Pivot Point on Airfoil Dynamic Stall," AIAA Paper 85-0130, Jan. 1985.

[10]Walker, J. M. and Chou, D. C., "Forced Unsteady Vortex Flows Driven by Pitching Airfoils," AIAA Paper 87-1331, 1987.

[11]Robinson, M., Helin, H., Gilliam, F., Russell, J., and Walker, J., "Visualization of Three-Dimensional Forced Unsteady Separated Flow," AIAA Paper 86-1066, May 1986.

[12]Strickland, J. H. and Graham, G. M., "Force Coefficients for a NACA 0015 Airfoil Undergoing Constant Pitch Rate Motions," *AIAA Journal,* Vol. 25, No. 4, 1987, pp. 622–624.

[13]Visbal, M. R., "Evaluation of an Implicit Navier-Stokes Solver for Some Unsteady Separated Flows," AIAA Paper 86-1053, May 1986.

[14]Visbal, M. R. and Shang, J. S., "Investigation of the Flow Structures Around a Rapidly Pitching Airfoil," *AIAA Journal,* Vol. 27, No. 8, 1989, pp. 1044–1051; see also AIAA Paper 87-1424, June 1987.

[15]Wu, J. C., Wang, C. M., and Tuncer, I. H., "Unsteady Aerodynamics of Rapidly Pitched Airfoils," AIAA Paper 86-1105, May 1986.

[16]McCroskey, W. J., McAlister, K. W., Carr, L. W., Pucci, S. L., Lambert, O., and Indegrand, R. F., "Dynamic Stall on Advanced Airfoil Sections," *Journal of the American Helicopter Society,* Vol. 26, No. 3, 1981, pp. 40–50.

[17]Bodapati, S. and Carr, L. W., "Compressibility Effects on the Dynamic Stall of Airfoils Undergoing Ramp-Type Motion," Workshop II on Unsteady Separated Flow, U. S. Air Force Academy, July 1987.

[18]Baldwin, B. and Lomax, H., "Thin Layer Approximation and Algebraic Model for Separated Turbulent Flows," AIAA Paper 78-257, Jan. 1978.

[19]Beam, R. and Warming, R., "An Implicit Factored Scheme for the Compressible Navier-Stokes Equations," *AIAA Journal,* Vol. 16, No. 4, 1978, pp.393–402.

[20]Steger, J., "Implicit Finite-Difference Simulation of Flow About Arbitrary Two-Dimensional Geometrics," *AIAA Journal,* Vol. 16, No. 7, 1978, pp. 679–686.

[21]Rubesin, M. and Rose, W., "The Turbulent Mean-Flow, Reynolds-Stress and Heat-Flux Equations in Mass-Averaged Dependent Variables," NASA TMX-62248, March 1973.

[22]Visbal, M. and Knight, D., "Generation of Orthogonal and Nearly Orthogonal Coordinates with Grid Control Near Boundaries," *AIAA Journal,* Vol. 20, No. 3, 1982, pp. 305–306.

[23]Visbal, M. R. and Shang, J. S., "Comparative Study Between Two Navier-Stokes Algorithms for Transonic Airfoils," *AIAA Journal,* Vol. 24, No. 4, 1986, pp. 599–606.

[24]Harris, C. D., "Two-Dimensional Aerodynamic Characteristics of the NACA 0012 Airfoil in the Langley 8-Foot Transonic Pressure Tunnel," NASA TM-81927, April 1981.

[25]Holst, T. L., "Viscous Transonic Airfoil Workshop Compendium of Results," AIAA Paper 87-1460, Jan. 1987.

[26]McCroskey, W. J., Carr, L. W., and McAlister, K. W., "Dynamic Stall Experiments on Oscillating Airfoils," *AIAA Journal,* Vol. 14, No. 1, 1976, pp. 57–63.

[27]Ericsson, L. E., "Review of Transition Effects on the Problem of Dynamic Simulation," AIAA Paper 88-2004, May 1988.

[28]Ericsson, L. E., "Dynamic Effects of Shock-Induced Flow Separation," *Journal of Aircraft,* Vol. 12, No. 2, 1975, pp. 86–92.